Topologically defined composites of collagen type I and V as *in vitro* cell culture scaffolds

Katja Franke[a,*], Jiranuwat Sapudom[a], Liv Kalbitzer[a], Ulf Anderegg[b], and Tilo Pompe[a]

[a]*Biophysical Chemistry Group, Institute of Biochemistry, Faculty of Biosciences, Pharmacy and Psychology, Universität Leipzig, Leipzig 04103, Germany*
[b]*Department of Dermatology, Venerology and Allergology, Universität Leipzig, Leipzig 04103, Germany*

**Corresponding author. Institute of Biochemistry, Faculty of Biosciences, Pharmacy and Psychology, Universität Leipzig, Leipzig 04103, Germany. phone/fax: ++49 341 9736-932/939.*
E-mail address: katja.franke@uni-leipzig.de

This article was published in final edited form as:

Franke K, Sapudom J, Kalbitzer L, Anderegg U, Pompe T. Topologically defined composites of collagen types I and V as in vitro cell culture scaffolds. Acta Biomater 10:2693-702 (2014).

Abstract
Cell fate is known to be triggered by cues from the extracellular matrix including its chemical, biological and physical characteristics. Specifically, mechanical and topological properties are increasingly recognized as important signals. The aim of this work was to provide an easy-accessible biomimetic *in vitro* platform of topologically defined collagen I matrices to dissect cell behaviour under various conditions *in vitro*. We reconstituted covalently bound layers of three-dimensional (3D) networks of collagen type I and collagen type V with a defined network topology. A new erosion algorithm enabled us to analyse the mean pore diameter and fibril content, while the mean fibril diameter was examined by an autocorrelation method. Different concentrations and ratios of collagen I and V resulted in pore diameters from 2.4 µm to 4.5 µm and fibril diameters from 0.6 to 0.8 µm. A comparison of telopeptide intact collagen I to telopeptide deficient collagen I revealed obvious differences in network structure. The good correlation of the topological data to measurements of network stiffness as well as invasion of human dermal fibroblasts proofed the topological analysis to provide meaningful measures of the functional characteristics of the reconstituted 3D collagen matrices.

Keywords
collagen structure, topology, image analysis, mechanical properties, fibroblast

1. Introduction

The complex interactions of cells with their microenvironment affect cell fate decisions *in vivo* as well as *in vitro*. These phenomena include mechanical contact with the extracellular matrix (ECM), binding of immobilized and dissolved signalling molecules and direct interactions with neighbouring cells. The biochemical and biophysical cues of the ECM, in particular the type of ligand, ligand density, their spatial distribution (2D versus 3D), matrix topology and orientation as well as matrix stiffness and viscosity are currently discussed as important parameters to control cell fate decisions [1-3]. Recent reports emphasize the importance of 2D and 3D distributions of ECM ligands in affecting cell morphology, proliferation, differentiation and apoptosis [4, 5]. Especially, 3D scaffolds were shown to distinctively alter cell behaviour to a more *in vivo* phenotype in comparison to standard 2D culture systems [5, 6].

To understand the underlying regulatory mechanisms, there is a need for advanced *in vitro* assays that mimic *in vivo* microenvironments but limit the overwhelming complexity therein. In order to modulate the topology and mechanical properties of ECM scaffolds two main approaches are followed: synthetic *and* natural matrices. Many efforts established synthetic hydrogels as cell culture scaffolds [7-9]. Within this approach, the introduction of small synthetic peptides like RGD within these scaffolds is increasingly used as a substitute of native protein ligands [10, 11]. Beside the highly reproducible chemical quality of *synthetic* materials, a major drawback is their lack of specificity, decreased receptor binding affinity and synergistic functionality [2, 12]. In contrast, other research focuses on the application of decellularized ECM of intact mammalian tissues as a scaffold for tissue engineering bearing the advantage of a complex *natural* composition and topology [13]. The unknown complex composition and immunologic side effects constitute a major drawback in this approach. Matrigel, as another prominent example of natural matrices [14, 15] has similar consequences of a mostly undefined composition and difficulties to dissect cell-ECM interactions.

Approaches at an intermediate level between synthetic and decellularized scaffolds use defined matrices based on natural ECM proteins. Reconstituted 3D collagen [16, 17] or fibrin networks [18] are applied as various cell culture scaffolds, e.g. as support of vascularization of tissues [19]. Fibril-forming collagens i.e. type I, III, V, XI, XXIV and XXVII are interesting candidates for reconstitution of a bio-analogue 3D ECM *in vitro*. The ECM of the skin for instance mainly consists of collagen type I (Coll I) in co-assembling with collagen type III and lesser amounts of collagen type V (Coll V). In contrast, cornea is constructed from Coll I and higher amounts of Coll V [16]. The varying amounts of Coll V found in different tissues suggest a role in modulating the structure of collagen fibrils. Tissues with less Coll V contain fibrils with larger and more variable diameter, whereas the fibril diameter of matrices with high levels of Coll V is small and tightly controlled [20]. Additionally, different collagens were found to co-assemble into banded fibrils [16]. However, it is unclear whether a heterotypic supercoiled structure is formed or if the molecules are buried within the fibrils [21]. Cells use Coll V and collagen type XI to nucleate Coll I fibrils, while fibronectin is used to instruct the fibril assembly by using specific collagen binding sites [22, 23]. Although these collagen structures are frequently found *in vivo,* only a few studies on *in vitro* matrix engineering address the co-assembly of different types of collagens. Piechocka et al. [24] reconstituted matrices using Coll I and V to investigate the influence of collagen composition on the network structure and rheology. As a result, the network stiffness decreased with increasing content of Coll V with no remarkable changes in the fibril diameter. Many other studies use solely Coll I to engineer different ECM properties by varying pH, salinity, temperature, collagen sources and concentration during fibrillogenesis [25-29]. By comparing commercially available collagens from different species including preparations of pepsinized and non-pepsinized Coll I and different self-assembly conditions, the *in vitro* reconstituted collagen networks have remarkable differences regarding pore size and fibril morphology. It was demonstrated that the characteristic homogeneous structure of *in vitro* reconstitutions of pepsinized and non-pepsinized collagen with a mean pore area of 2 and 15 μm^2, respectively, at 1.7 mg/ml is not found inside *in vivo* tissues, which exhibit pore areas from 10 to 1000 μm^2 [28].

Because of the extensive use of collagen to generate 3D cell culture scaffolds and the importance of the physical parameters of ECM to regulate cell behaviour, there exist several approaches to analyse the topology of reconstituted networks. Image analysis algorithms based on microscopic investigations become a powerful strategy for the topological characterization of collagen-based networks. Collagen fibril reconstitution is performed either in presence or in absence of fluorescent-labelled tropocollagens. Subsequently, collagen networks are typically investigated either by second harmonic generation microscopy (SHG) [30-32], confocal reflection microscopy (CRM) [33, 34], scanning electron microscopy (SEM) [32, 35, 36], transmission electron microscopy (TEM) [36] and confocal fluorescence microscopy (CFM) [34, 37-39]. Studies comparing CRM and SHG to CFM reveal a higher fidelity of the 3D network topology reconstructed from CFM images [34, 40] as collagen fibrils oriented above a cut off angle to the imaging plane cannot be detected by CRM [40, 41]. A drawback of fluorescence labelling of tropocollagen prior to fibrillogenesis is the possible impact of the fluorescent label on the structure and mechanics of the reconstituted collagen networks [34]. SHG two-photon microscopy demonstrated a more accurate fibril detection than fluorescence-based methods [32]. SEM and TEM analysis require scaffold processing and drying which modifies the collagen networks. In this regard the broad spectrum of microscopy tools needs a critical examination with respect to pros and cons on the required network modifications as well as the microscopic accuracy.

To reveal the collagen network topology from the microscopic analysis, i.e. the pore size, frequently manual measurements are applied which are time consuming and lack statistical significance. Only a few automated approaches exist mainly based on iterative algorithms or probability calculations to determine pore or mesh size of collagen networks. Iterative methods randomly select a point and its associated largest sphere touching the nearest collagen fibril in the pore space. Subsequently, the point position is adapted until the sphere fits the surrounding fibrils [42]. The usage of probability calculations is based on a density-function to gain the pore-size probability [43]. Fibril diameter and orientation inside collagen networks were analysed by several methods including ellipse fitting method [31], two-dimensional Fourier transformation [30] and grey level analysis along a search line [35]. Possible image analysis methods considerably differ in time consumption and accuracy and strongly depend on the quality of source images.

In this report, topologically defined 3D collagen matrices are engineered and characterized. A newly developed image analysis algorithm based on CFM data performs the topological characterization of 3D collagen matrices, e.g. pore size, fibril diameter and fibril content. Correlation of the topological data to mechanical measurements and cell invasion studies demonstrates the applicability of the approach.

2. Materials and Methods

2.1 Covalent collagen network immobilization

For a covalent immobilization of collagen networks onto stable carriers we prepared thin coatings of poly(styrene-*alt*-maleic anhydride) (PSMA) as published elsewhere [44]. Briefly, a 0.14% (w/w) PSMA-copolymer (MW 20000-30000) solution in acetone (AppliChem, Darmstadt, Germany) and tetrahydrofurane (AppliChem) at a ratio of 1:2 was spin-coated onto pre-cleaned and amine-functionalized glass coverslips of 13 mm diameter (VWR international, Leuven, Belgium). The presence of anhydride groups during the collagen fibril formation enables a covalent collagen-surface binding by lysine side chains. For a sketch of the setup, see Figure 1.

2.2 Collagen network reconstitution

All preparations of 3D collagen networks were performed at identical conditions. Collagen solutions were diluted in 1× phosphate buffered saline (PBS, Biochrom, Berlin, Germany) and neutralized with 10× PBS and 0.1 N NaOH (Diagonal, Münster, Germany). Final collagen concentrations ranged from 1 to 2.8 mg/ml. Networks reconstituted from Coll I with telopeptides (rat tail, BD Bioscience, Heidelberg, Germany) were limited to concentrations of 2.8 mg/ml and atelo Coll I (bovine, Nutacon BV, Leimuiden, Netherlands) to 2.0 mg/ml. Networks with mixtures of Coll I and Coll V (human, Sigma

Aldrich, Munich, Germany) were prepared at 20%, 35% and 50% content of Coll V at a final collagen concentration of 2 mg/ml. Neutralized collagen solutions were kept on ice prior to the induction of fibrillogenesis by warming to 37 °C within 90 min. For topological and mechanical analysis of the collagen networks as well as for cell invasion experiments fibrillogenesis was performed on PSMA-coated glass coverslips using 20 µl of neutralized collagen solutions. The reconstituted networks were strictly kept in a hydrated state to avoid artefacts by drying and aggregation.

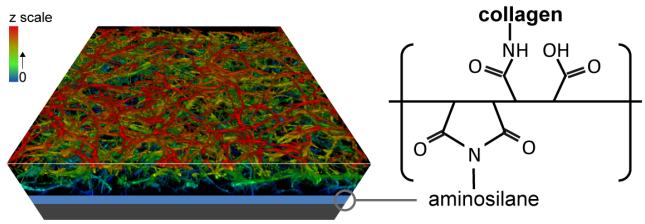

Figure 1.
Setup of covalently bound collagen scaffolds and 3D projection of a reconstituted collagen I network. Cover glasses are modified using maleic anhydride co-polymers by thin-film coating. Collagen fibrillogenesis in the presence of reactive anhydride groups enables a covalent binding of native collagen scaffolds via lysine side chains.

2.3 Analysis of network topology

For analysis of the network topology we investigated 6 samples per experimental condition using a confocal laser scanning microscope (LSM 780) and a 63× oil immersion objective (both Zeiss, Jena, Germany). Prior to microscopy the reconstituted networks were labelled with 50 µM carboxytetramethylrhodamine (TAMRA, Sigma Aldrich) overnight at room temperature with a subsequent rinsing three times in PBS and embedding on glass slides using Eukitt® (Diagonal). 16-bit images at a xy-size of 1024×1024 pixels and a vertical stack size of 80 images, equivalent to 40 µm, were typically taken near the substrate surface. The resulting voxel size of the images was 0.13×0.13×0.5 µm (x×y×z). Total layer thickness was evaluated in the CFM investigations by the vertical difference between the surface of the glass substrate and the top surface of the collagen network using a 10× dry objective (Zeiss).

The newly developed automated algorithm for image analysis (using MATLAB (MathWorks, USA)) consists of 4 major steps and is applied to each xy-image of the image stack: I) automated image segmentation into pore and fibril segments, II) calculation of the mean pore diameter by an erosion algorithm, III) evaluation of the mean fibril diameter by autocorrelation, and IV) calculation of the fibril content. An extended explanation of the algorithm of the automated topology analysis, is found in the Supplementary data including a work flow of image processing and analysis of pore diameter, fibril diameter and fibril content (Supplementary Figure S1).

In brief, automated image segmentation (I) applies a binary transformation of original CFM images by thresholding, see Figure 2A and Supplementary Figure S2. Pixels with an intensity above the median value of the xy-image were set to 1 (pore) and pixels with the mean intensity and below were set to 0 (fibril). Thereafter, edge-smoothing using non-linear filtering (mean values of neighbouring 3×3 pixels) removed remaining noise in segmented images. The accuracy of binary image transformation is depicted in Supplementary Figure S2. The erosion algorithm (II) randomly fills up all segmented pores with circular disks of a predefined diameter (1 to 15 µm), see Figure 2B. The number of disks results from all possible disk placements within each single pore ensuring a spatial confinement within the contour of the segmented pores. The eroded pore area depends on the disk diameter. We take the value of the mean pore diameter of the network at 50% of the total pore area, see Figure 2C. A visualization of the erosion of total pore area by the varying disk diameter is provided in Supplementary Figure S3, too.

The mean fibril diameter D_{fib} is calculated similar to the approach published elsewhere [29] using an

autocorrelation analysis with small improvements, see below and Figure 3B. The 2D autocorrelation function $C(i,j)$ is usually applied to assess a randomly or directional alignment of structures within an image (e.g. fibril orientation). It is calculated from the intensities I of the images of size $M \times N$ pixels by:

$$\mathrm{C}(i,j) = \frac{1}{NM}\sum_{m=1}^{M}\sum_{n=1}^{N} I(m,n)\cdot I(m+i,n+j) \Big/ \left[\frac{1}{NM}\sum_{m=1}^{M}\sum_{n=1}^{N} I(m,n)\right]^2 - 1$$

with i and j being the separation distance in pixels in x and y direction. We now fit a rotating 2D Gaussian

$$C'(i,j) \cong C'(0,0)e^{-\left(\left((i\cdot cos(\theta)+j\cdot sin(\theta))/2\sigma_1\right)^2+\left((-i\cdot sin(\theta)+j\cdot cos(\theta))/2\sigma_2\right)^2\right)} + C'_0$$

to the central 128×128 pixels of $C(i,j)$ and take the smaller value of $2\sigma_1$ and $2\sigma_2$ as D_{fib}, with $2\sigma_1$ and $2\sigma_2$ being the two independent width of the 2D Gauss function in the xy-plane at 68% of $C'(0,0)$. C'_0 is the background offset, while θ depicts to free rotation angle of the 2D Gaussian in the xy-plane. The rotating 2D Gaussian fit was performed using the *fit* command within Curve Fitting Toolbox, resulting in a surface fit to the xyz data, whereby x and y were set as independent variables and z as dependent variable. The fibril diameter was averaged over the stacked image. Choosing the Gaussian fit with variable σ in two axes and free rotation allows for a better analysis of non-isotropic effects of fibril orientation and a more meaningful analysis of the fibril diameter as the smallest relevant length scale in the image. The fibril content (IV) as an additional network parameter was estimated by counting black and white pixels out of the segmented image.

For the validation of the algorithm, see results section *3.1 'Validation of the automated image analysis'*, phantom images were generated from binary model images with disks and lines of defined diameter and width, respectively, to simulate pores and fibrils of a collagen network (Figure 3A and B) using Adobe Photoshop CS5 (Adobe System Inc., USA). Lines varied in width of 20 and 40 pixel and disks varied in diameter between small (100 pixel), middle (200 pixel) and large (300 pixel). The porosity of each phantom image, equal to the total pore area, was constant, whereas the ratio of the different disk diameter varied (Figure 3A). Phantom images were 1024×1024 pixel in resolution.

2.4 Kinetic study of fibrillogenesis

Neutralized collagen solutions were prepared at 1, 2 and 2.8 mg/ml if not stated otherwise. 100 µl of each collagen concentration were transferred into pre-chilled (4°C) 96-well plates prior to fibrillogenesis. Plates were loaded into a pre-warmed (37°C) plate reader (Tecan Infinite F200Pro, Tecan, Grödig, Austria) and optical density at 405 nm was measured at 1 min intervals for 4 h. Measurements were performed in at least three independent experiments.

2.5 Quantification of non-fibrillar collagen content

The concentration of non-fibrillar collagen after fibrillogenesis was determined in supernatants by Bradford assay. 300 µl of neutralized collagen solution was prepared and fibril formation was performed at 37°C for 90 min in tubes (Eppendorf, Wesseling-Berzdorf, Germany). Fibrils were separated by centrifugation (2-16PK, Sigma, Osterode am Harz, Germany) for 15 min at 4°C and 10000 g according to the method previously reported [45]. Supernatant and pellet were separated and retained at 4°C for subsequent analysis. 20 µl of supernatant was mixed with 180 µl Bradford reagent and incubated for 10 min at room temperature. Subsequently, the absorbance was measured at 595 nm using a Power Wave XS universal microplate spectrophotometer (BIO-TEK Instrument Inc., Vermont, USA). A calibration curve was derived from solutions of the respective collagen type ranging from 0 to 2 mg/ml. All experiments were performed in triplicates.

2.6 Colloidal probe force spectroscopy of 3D collagen networks

A Nanowizard III AFM (JPK Instruments, Berlin, Germany) was used for performing colloidal probe force spectroscopy of the 3D collagen networks. The colloidal probes were prepared by attaching a 15 µm polystyrene microbead (Polyscience Europe GmbH, Eppelheim, Germany) to a tipless MLCT triangular cantilever (Bruker AFM probes, Camarillo, CA) with a spring constant of approx. 60 nN/m. The exact spring constant was determined by the thermal noise method [46].

All measurements were performed in phosphate buffered saline (PBS, Biochrom, Berlin, Germany) at room temperature. At least 80 force-distance curves were measured for each collagen network preparation. The Young's modulus of the networks was evaluated from the force-distance curves by fitting the Hertz model for an indentation of 3 to 10 µm.

2.7 Analysis of cell invasion, migration and morphology

Primary human dermal fibroblasts from healthy donor after informed consent were isolated and cultivated in DMEM (Biochrom, Berlin) supplemented with 10% fetal calf serum and 1% antibiotics (Penicillin/Streptomycin, Biochrom) as published elsewhere [47]. Finally, 5×10^3 cells were seeded on top of substrate-bound collagen matrices placed in 24-well plates (Greiner, Bahlingen, Germany) and cultivated at 37°C, 95% humidity and 5% CO_2 atmosphere. Cell invasion was analysed after 5 days of culture. For analysis, cells were fixed in 4% paraformaldehyde (Roth, Karlsruhe, Germany) for 10 min, permeabilized with 0.1% Triton X100 (Roth) at room temperature for 10 min and incubated with DAPI (Invitrogen) for 30 min at room temperature and directly analysed for cell invasion.

Images were taken at 1388×1040 pixels in xy-size and 5 µm z-distance using a 10× objective on an AxioObserver.D1 with scanning stage (Zeiss). Z-positions of about 200-300 cells per data point were analysed using DAPI signal from individual cell nuclei. Cells found >10 µm below the collagen layer surface were counted as invasive cells. Experiments were performed in triplicates.

For analysis of the cell morphology, additional incubation with Alexa Fluor488 Phalloidin (Invitrogen, Freiburg, Germany) was performed after permeabilization to visualize the actin cytoskeleton. Samples were embedded on glass slides in PBS using Eukitt® and analysed using a confocal laser scanning microscope (LSM 780, Zeiss) with 40× oil immersion objective.

2.8 Statistical analysis

Experiments were usually done in at least three independent runs, if not otherwise stated. Results are represented as mean $\pm$ standard deviation. Significant differences between data sets were calculated using an unpaired t-test at a p-level of 5% using OriginPro 8 (OriginLab Corp.).

3. Results

3.1 Validation of the automated topology analysis

We developed an automated image analysis tool to examine the topology of 3D fibrillar networks i.e. pore diameter, fibril diameter and fibril content from image stacks taken by CFM. The new approach to determine the mean pore diameter of a 3D network using an erosion algorithm is depicted in Figure 2. In a first step, original CFM images are transformed into binary images by thresholding (Figure 2A (1) and (2)). The binary image is then converted into pore and fibril segments and an erosion of the total pore segment-area with disks of varying diameter reveals the mean pore diameter at 50% of eroded pore area. Figure 2A (3) exemplary visualizes the binary image with 50% of eroded pore area. For clarification, Figure 2B demonstrates the erosion of one drafted pore segment by two different disk sizes and in Figure 2C the eroded pore area is plotted depending on the disk diameter. More detailed information on the image binary transformation and subsequent segmentation are provided in Materials & Methods. A comprehensive work flow of the algorithm, the accuracy of binary image transformation and the principle of pore area erosion by varying disk diameter are described and visualized in Supplementary data.

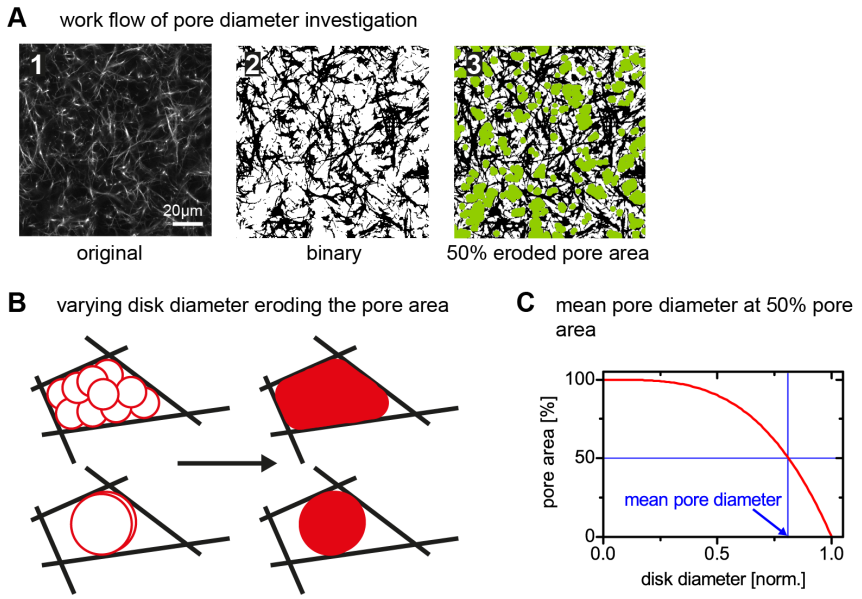

Figure 2.
Erosion method to determine the pore area. (A) Overview of work flow of the erosion algorithm. A binary image generated from an original image is eroded by the analysed mean pore diameter. (B) A network pore is exemplary shown and eroded by disks of increasing diameter (for clarity not all disks shown). While small-diameter disks fill the pore area to a large fraction, disks with large diameter only partly fill the pore area. (C) The eroded pore area in percent plotted above the increasing disk diameter. The disk diameter at 50% of total pore area is taken as the mean pore diameter.

To validate the algorithm we generated phantom images with defined parameters such as circle diameter and line width, see Figure 3A and B. The ratio of circle diameters was varied in each phantom image generating different numbers of small, middle and large circles in order to mimic various pore distributions in fibrillar networks. Corresponding diagrams in Figure 3A and B show results of the automated topology analysis and confirm the capability of the algorithm to determine the mean pore diameter and the mean fibril diameter with high precision. In a uniform phantom with only one pore diameter as well as in a phantom with an equal ratio of small, middle and large pores, the calculated mean pore diameter is exactly the implemented pore diameter or the diameter of the middle pore size. With a higher ratio of small or large pores, the erosion algorithm exactly determines the small or large pore diameter. The improved autocorrelation algorithm for the determination of fibril diameter precisely detects the correct fibril diameter in pure and mixed configurations from the smallest 2σ of the rotating Gaussian fit, see Figure 3B.

3.2 Topological analysis of the 3D collagen matrices

To test the applicability of our topological analysis we prepared a set of different matrices. We used Coll I from different preparations (acid-solubilized with telopeptides and pepsin-solubilized without telopeptides (atelo Coll I) and supplements of Coll V to modulate collagen network properties as these parameters are known to influence fibril self-assembly and intrafibrillar crosslinks. The Coll I concentration was varied from 1 to 2.8 mg/ml. The content of Coll V was adjusted between 20% to 50% at a total collagen concentration of 2 mg/ml.

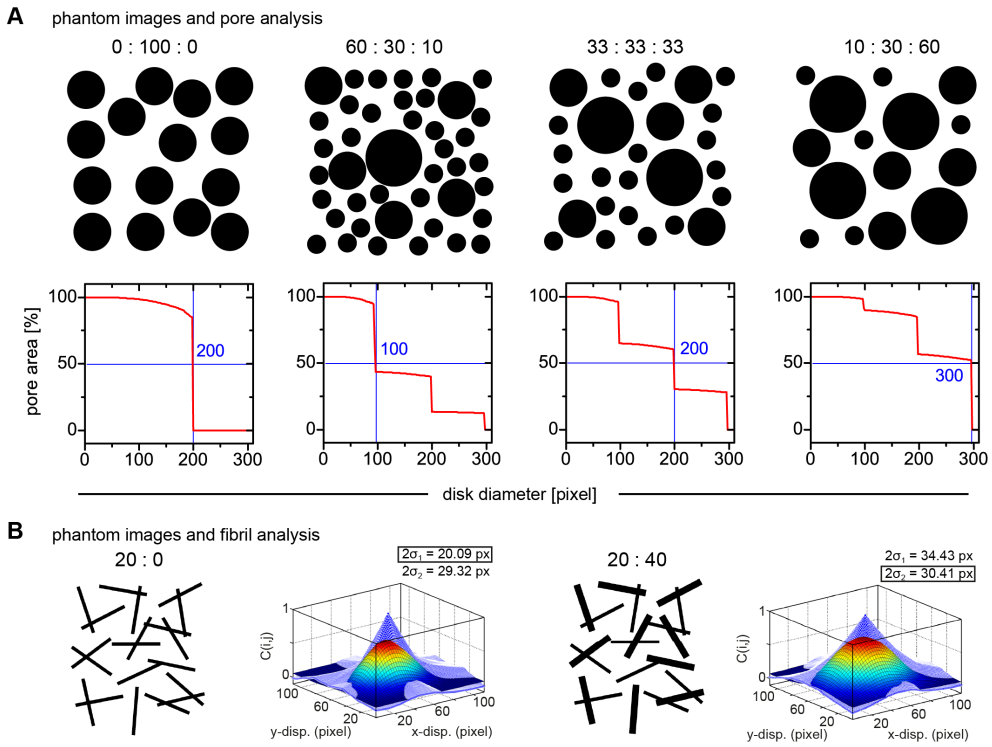

Figure 3.
Validation of the automated topology analysis by phantom images mimicking different pore size distribution and fibril diameter of a collagen network. (A) First row: Networks were simulated by circular pores of defined diameter e.g. small (100 pixels), middle (200 pixels) and large (300 pixels) and varying ratios of small : middle : large. The overall porosity (open area) of each phantom is constant. Corresponding graphs (below each phantom image) show the application of the new erosion algorithm to determine automatically a mean pore diameter. (B) Lines with a defined width (20 pixels (left phantom) and a 1:1 ratio of 20 and 40 pixels (right phantom)) and random orientation mimic the collagen fibrils. The algorithm calculates a fibril diameter from the minimal 2σ of the rotating 2D Gaussian fit of the autocorrelation function $C(i,j)$.

At first, the visual inspection of image stacks from CFM investigations indicated general trends. Figure 4 exemplarily shows networks of Coll I and atelo Coll I of different concentration and varying content of Coll V. As expected, the network density increased with increasing Coll I concentration (Figure 4A - C). A content of 50% Coll V does not influence the network density (Figure 4B and D), which is in agreement with the optical density (OD) analysis (data not shown). Networks reconstituted from atelo Coll I exhibited a more loose structure with thinner and shorter fibrils, see Figure 4E. Interestingly, in case of atelo Coll I the presence of Coll V (20%, Figure 4F) enhanced the network connectivity as well as the fibril length and thickness. However, when analysing the homogeneity of atelo Coll I networks even in combination with Coll V we found a slight gradient in the fibril structures with a high fibril content near the substrate surface and a low fibril content at the top surface of the layer. In contrast, collagen matrices reconstituted from telopeptide containing Coll I and Coll I/V revealed a high homogeneity in fibril content and pore diameter from bottom to top. Figure 5 depicts the homogeneity of different collagen matrices in vertical direction concerning fibril content (A) and mean pore diameter (B). For all matrices (telopeptide containing and atelo Coll I networks as well as networks containing Coll V) a homogenous distribution of mean pore diameters is found throughout the matrices, indicating a reliable preparation procedure of the collagen networks.

To ensure no impact of a varying thickness of the collagen layers on cell culture experiments [48] we checked the total layer thickness of the collagen matrices in the CFM measurements. In general, we found a layer thickness between 170 – 190 µm for Coll I preparations, while atelo Coll I matrices were

slightly thinner with roughly 130 – 150 µm. There was a slight tendency of thinner layers with increasing Coll V content.

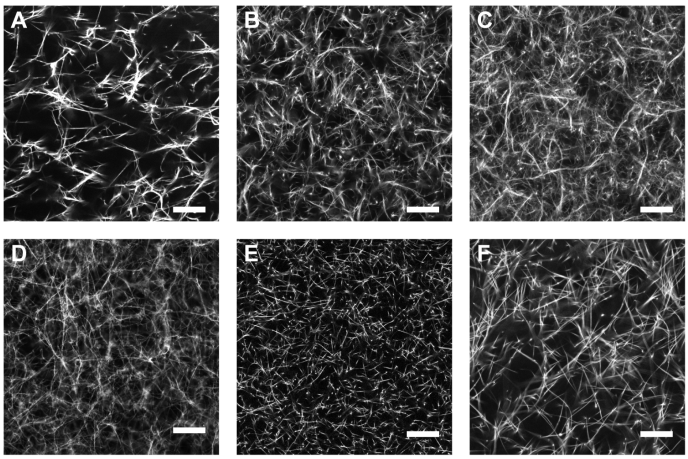

Figure 4.
Collagen networks reconstituted from different types of collagen. A variety of images of collagen networks investigated by CFM is exemplary shown. (A) 1 mg/ml Coll I, (B) 2 mg/ml Coll I, (C) 2.8 mg/ml Coll I, (D) 50% Coll V at 2 mg/ml Coll I/V, (E) 2 mg/ml atelo Coll I, (F) 20% Coll V at 2 mg/ml atelo Coll I/V. Scale bar 20 µm.

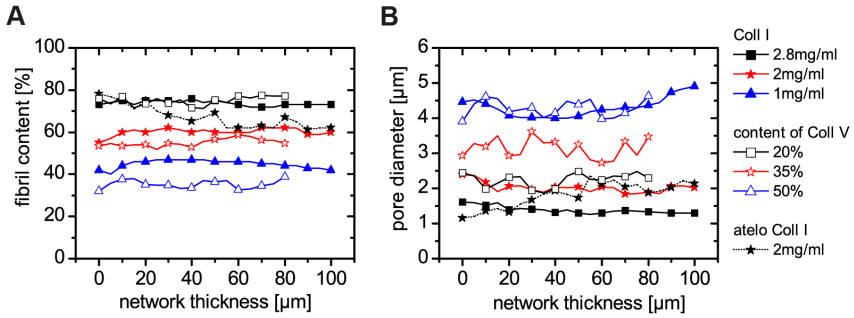

Figure 5.
Homogeneity of the fibril content and the pore diameter throughout the network. Mean values of fibril content (A) and pore diameter (B) throughout a network segment of 80 or 100 µm in z-direction were determined by automated topology analysis of confocal image stacks. Typical data are shown for networks reconstituted at 1, 2 and 2.8 mg/ml Coll I (solid line, filled symbols); Coll I networks at 2 mg/ml containing 20 - 50% Coll V (solid line, blank symbols); and atelo Coll I at 2 mg/ml (dotted line, filled symbol).

As next, we quantitatively analysed the topological parameters, namely pore diameter and fibril diameter. For both, Coll I and atelo Coll I (Figure 6A and 6B), the pore diameter can be adjusted over a wide range, while the fibril diameter is maintained at a nearly constant value. The increase in Coll I concentration from 1 to 2.8 mg/ml leads to a decrease in pore diameter from 4.5 µm to 1 µm, see Figure 6A. A high content of Coll V (35% and 50%) at 2 mg/ml of total collagen concentration leads to a significant increase of the pore diameter from about 2.5 µm (0% and 20%) to 4.5 µm (at 50%). No significant difference of the pore diameter at 50% content of Coll V was found comparing the pore diameter at 1 mg/ml Coll I. Analysis of the pore diameter of Coll I and atelo Coll I revealed no significant differences at 2 mg/ml collagen concentration with a pore diameter of about 2 µm. However, a visual comparison of these two networks in Figure 4B and 4E indicated a different network topology (atelo Coll I having loose structures with thinner and shorter fibrils compared to Coll I). Remarkable our analysis can also reveal these differences, when plotting the full range of the pore diameters eroding

the pore area, see Figure 6C. This distribution of pore diameters reflects the shift in details of the network topology. While atelo Coll I exhibited a narrow distribution of eroding pore diameters, 1 µm to 5 µm, Coll I exhibited a broader range of 1 µm to almost 10 µm. Hence, we can conclude, that although the mean pore diameter give a good measure for the network topology, in-depth analysis provides additional information for correlation to functional studies, e.g. mechanical properties and cell culture.
The fibril diameter was found to be almost constant for all samples with values of approx. 800 nm for Coll I. Only preparations with high content of Coll V (50%) and atelo Coll I matrices resulted in smaller fibril diameters of approx. 600 nm. As expected, fibrils are randomly and isotropically oriented within the networks, which can be concluded from the autocorrelation analysis.
We further analysed the fibril content to validate the trends of pore area and fibril diameter in the context of the overall network porosity (data not shown). As it can be expected from the almost constant fibril diameter, the fibril content was found to correlate with the pore diameter. Networks with a high pore diameter exhibit a low fibril content and vice versa.

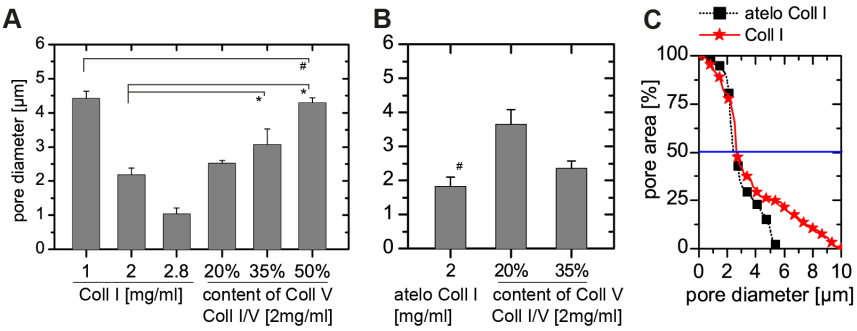

Figure 6.
Comparison of the mean pore diameter and pore diameter distribution in collagen networks. Automated topology analysis reveals the pore diameter of Coll I (A) and atelo Coll I (B) alone and in combination with a defined content of Coll V. Distributions of pore diameter eroding the pore area of Coll I and atelo Coll I networks at 2 mg/ml are exemplary shown (C). The blue line indicates the mean pore diameter at 50% eroded pore area. Mean values +SD are calculated out of topology analysis of at least 3 independent experiments. Unpaired t-test at 0.05 level revealed significant (*) differences comparing pore diameter of Coll I at 2 mg/ml to Coll I at 2 mg/ml with varying amount of Coll V (20%, 35% and 50%). The pore diameter comparing Coll I at 1 mg/ml to Coll I at 2 mg/ml with a content of 50% Coll V and comparing Coll I at 2 mg/ml to atelo Coll I at 2 mg/ml was not significantly different (#).

3.3 Further characterization of fibrillogenesis and collagen networks
Besides the topological analysis, we investigated the kinetics of fibrillogenesis, the remaining amount of non-fibrillar collagen after fibrillogenesis and the stiffness of collagen networks in order to better control the conditions of the preparation of the collagen networks and to test the correlation of these parameters to the topological data.
We examined the kinetics of fibrillogenesis at 37°C and pH 7.4 by OD measurements at 405 nm to obtain information on collagen fibrillogenesis and to correlate the nucleation and kinetics with the network topology, see Figure 7A. In general the results are in agreement with the existing knowledge on collagen fibrillogenesis [16]. After the lag phase of fibril nucleation samples for Coll I and atelo Coll I reached the same OD at identical collagen concentrations. The lag phase shortened with increasing collagen concentration due to the higher probability of promoting nucleation of fibrils. Atelo Coll I at 2 mg/ml showed a significant retardation of fibrillogenesis (60 min compared to 12 min) due to the absence of telopeptides that are known to support early aggregation of tropocollagen. This effect was compensated by the presence of Coll V known to nucleate collagen fibrils *in vivo* [22, 23]. This finding points to a similar function as nucleator in the presented *in vitro* system, although the impact of Coll V was only observed for the relatively slow fibrillogenesis of atelo Coll I (data not shown).

The kinetic results were supported by the analysis of non-fibrillar collagen in the supernatant after fibril formation. The percentage of non-fibrillar collagen in relation to the initial amount of collagen increased with increasing Coll V content (0% to 50%) from 0.8% to 12%, see Figure 7B. Also the disturbed fibril formation of atelo Coll I (layer thickness, lag phase, heterogeneity) was reflected in a higher amount of non-fibrillar collagen in the range of 17.7% to 23.8% in comparison to telopeptide intact Coll I. These results correlated with the slightly smaller layer thickness at increasing Coll V content, see above. It is further in line with the larger pore diameter at higher Coll V content, see Figure 6A pointing to an impaired efficacy of collagen fibrillogenesis at high Coll V content.
Furthermore, we used colloidal probe force spectroscopy to investigate the micromechanical properties of the collagen networks. The results of three different matrices, Coll I at 1 mg/ml and 2 mg/ml as well as Coll I with 20% Coll V at 2 mg/ml were measured, see Figure 8A. As expected from the topology analysis the Young's modulus decreased with a lower collagen concentration from 19 Pa to 8 Pa in good correlation to an increase in mean pore diameter for these matrices. This is similar true for the heterotypic matrix with 20% Coll V showing similar Young's moduli in correlation to similar pore diameters. Interestingly, the spreading of data was much narrower for the heterotypic indicating an influence of Coll V as nucleator of fibril assembly leading to a more homogenous fibril distribution.

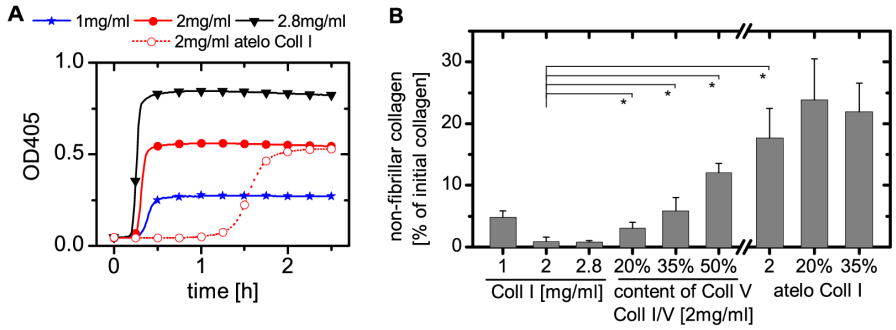

Figure 7.
Kinetic studies of fibrillogenesis and analysis of remaining non-fibrillar collagen content. (A) Fibrillogenesis of telopeptide containing Coll I at varying concentration from 1 to 2.8 mg/ml and of atelo Coll I at 2 mg/ml was analysed by optical density measurements at 405 nm. A typical experiment out of 3 independent experiments is shown. (B) Non-fibrillar collagen content of Coll I compared to atelo Coll I in dependence on concentration and varying content of Coll V as determined after fibrillogenesis. The non-fibrillar collagen protein amount in the supernatant is shown in percent of total employed collagen. Mean value +SD of 3 independent experiments are shown. Significant differences of non-fibrillar collagen amounts were proofed comparing Coll I samples containing 20%, 35% and 50% Coll V as well as atelo Coll I at 2 mg/ml to Coll I at 2 mg/ml (*) using an unpaired t-test at 0.05 level.

3.4 Topological and mechanical control of cell invasion

The engineered collagen matrices are intended for usage in *in vitro* cell assays mimicking a 3D cellular microenvironment. In order to demonstrate the possibility to correlate the quantitative topological analysis with cell behaviour we cultured primary dermal fibroblasts on three different collagen matrices. The cell type was chosen as it was envisioned to show mesenchymal migration characteristics sensitive for the network topology, which dictates the network mechanics likewise [49, 50]. The collagen networks were chosen by the topological data in order to have a set of matrices with different topology at similar composition and a set of matrices with similar topology at different composition. For this purpose we used Coll I matrices with 1 and 2 mg/ml and a network consisting of Coll I and 20% Coll V at a final concentration of 2 mg/ml. While the latter ones (Coll I, Coll I / 20% Coll V, both at 2 mg/ml) had a quite similar topology with a pore diameter of about 2 µm and a fibril diameter of 0.8 µm, Coll I matrices at 1 mg/ml exhibit larger pore diameter of 4.5 µm at a similar fibril diameter.

Cell invasion after 5 days of cell culture was evaluated as a straightforward parameter to access cell-matrix interaction in dependence on topology and mechanics. We quantified the number of cells which invaded the matrix at least 10 µm. As shown in Figure 8B, cell invasion reflects the differences in matrix properties. In comparison to Coll I at 2 mg/ml with 12% invasive cells, dermal fibroblasts have drastically reduced invasion characteristics on Coll I matrices at 1 mg/ml with only 1.4% invaded cells. This behaviour reflects the correlation of matrix topology and matrix mechanics. The stiffer matrices with the smaller pore diameter (2 mg/ml) better withstand cellular traction forces of the invading fibroblasts leading to a higher invasion efficacy as it would be expected from a mesenchymal migration type. The spindle shaped cell morphology, exemplarily shown in Figure 8C, supports the argument of a mesenchymal migration characteristic. The behaviour of dermal fibroblasts on heterotypic collagen matrices (Coll I/Coll V) shows an intermediate invasion potential (5% of the total cell number) which is again correlated to the intermediate stiffness of those matrices, see Figure 8A.

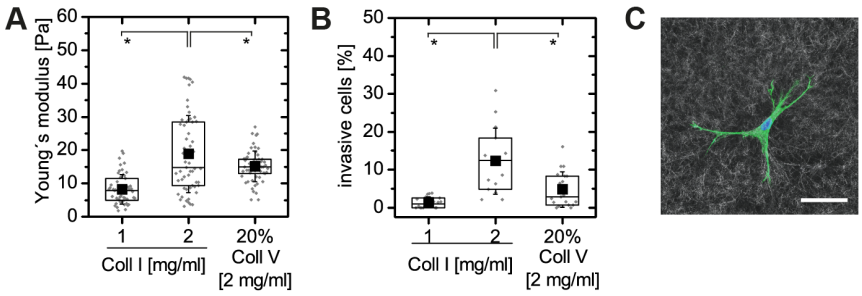

Figure 8.
Mechanical properties and cell invasion of selected matrices. (A) Micromechanical analysis of the collagen networks exhibit differences between matrices at 1 and 2 mg/ml (8 and 19 Pa) and a slight decrease in matrices containing 20% Coll V (15 Pa). (B) Networks at 1 and 2 mg/ml Coll I and 20% Coll V at 2 mg/ml enable invasion of primary fibroblasts after 4 days to a different extent in correlation to network mechanics and topology. (Boxes in (A) and (B) show the 25th and 75th percentile, whiskers indicate the standard deviation and black squares give the mean values of 3 independent experiments.) (C) A typical cell morphology on Coll I matrices at 2 mg/ml is shown from CFM. The spindle shaped cell with long filopodia indicate a typical mesenchymal behaviour. Significant differences of mechanical properties and cell invasion were observed comparing Coll I at 1 mg/ml and Coll I at 2 mg/ml containing 20% Coll V to Coll I at 2 mg/ml (*) using an unpaired t-test at 0.05 level. Scale bar 50 µm.

4. Discussion

Fundamental knowledge in cell-ECM interaction is required to either reveal, predict or control cell behaviour for applications in regenerative medicine or tissue engineering. The *in vitro* reconstitution of well-defined cellular microenvironments using artificial or natural materials is a promising tool to improve our understanding in cell behaviour. Advantageously, engineered matrices need to be 3D with a defined composition, stiffness, and topology, as these parameters are known to significantly influence cell behaviour. Within this study, we introduce a new erosion method within an image analysis algorithm to reveal the topology of fibrillar and porous 3D matrices. This strategy allowed us to characterise the topology of 3D scaffolds at high throughput and precision. Topological properties of substrate-bound collagen scaffolds were varied by controlling collagen composition and concentration leading to modulated fibrillogenesis, mechanics and cell invasion of these collagen networks.

With respect to the isotropic fibril orientation in a 3D collagen network which was found in this study (data not shown) and by others [29, 30, 40], the determination of the mean pore diameter using the introduced erosion method on 2D images is assumed to be a good measure of the 3D network topology. Our straightforward algorithm allows the analysis of a stack size of 100 images with 1024×1024 pixels within 2 min using a standard PC (Intel Core i5, 8 GB RAM). Topology analysis from 3D network

segments would enhance the time for image acquisition, 3D image reconstruction and topological analysis to a high extend while the gain on information depth would be modest. Other methods for pore size analysis are prone to misinterpret the pore structure when using only the maximal sphere radii [39, 42]. Furthermore, when fibril diameter or pore diameter are investigated manually as frequently done [51], the analysed network topology compromised by subjective decisions and the limited amount of data. Additionally, these methods would be time consuming. It has to be noted, that different types of networks and matrices can be analysed using the developed algorithm as it is simply based on a stack of grey scale images, which have to be binarized for further analysis.

We defined the mean pore diameter at 50% eroded pore area of the total one. We expect this measure together with fibril diameter and fibril content as a meaningful equivalent to the overall porosity of the scaffold or mesh size of the network. The mean pore diameter defined in that way provides a characteristic number to be correlated to the cross-section of an invading cell and mechanical properties of the network. Additionally, we could show that our analysis provides information on pore size distributions if needed, see Figure 6C.

It is important to note that the sensitivity of our method relies on the image resolution and on errors generated by the point-spread-function of the microscope. In particular, the fibril diameter is expected to be overestimated in our approach due to the optical resolution being in the similar range as the fibril diameter. Besides that, the used binarization was shown to maintain relevant image information and the improved autocorrelation method to more precisely determine fibril diameter than a circular 2D Gaussian fit.

The process of collagen fibril formation is highly sensitive to any additional molecule present during fibrillogenesis and strongly dependent on temperature, pH and salt concentration. For this reason, we omitted any addition of cell culture media, serum or fluorescent dye during fibrillogenesis and kept all physical and chemical parameters constant. Furthermore, to circumvent artefacts during the analysis of network topology and cell experiments we kept the reconstituted collagen networks in hydrated state. As topological analysis by CRM is not suitable to detect all collagen fibrils [40, 41] we fluorescently labelled the reconstituted 3D collagen networks subsequent to reconstitution for the investigation by CFM.

The quantitative analysis of the topology of the investigated collagen matrices allowed us to draw conclusions in respect to the engineering of defined network topologies of collagen matrices for cell experiments. Within our experimental setup we can adjust the pore diameter at an equal fibril diameter by varying the collagen concentration. Since the atelo Coll I preparations frequently exhibited heterogeneities we would not recommend to use atelo Coll I for *in vitro* 3D network reconstitution. Compared to *in vivo* situations the content of Coll V used herein (20 – 50%) is quite high since only about 10 – 12% Coll V was found in bovine cornea [52]. However, we demonstrated that for a matrix engineering approach the formation of collagen networks is possible even at high Coll V content. By a variation of Coll V content we can vary the resulting pore diameter at a constant fibril diameter in agreement with earlier reports [24]. We can engineer a similar network topology of about 4.5 µm pore diameter using different network compositions of 2 mg/ml Coll I/V at 50% in comparison to 1 mg/ml Coll I. Our results reveal that telopeptide intact Coll I does not need a trigger to initiate fibrillogenesis at high collagen concentrations, which are dominated by an entropy-driven self-assembly [22]. The data support earlier reports, that Coll V only acts as a nucleator, but cannot form fibrils itself [16, 17].

Our results agree with other studies on mechanical properties of heterotypic collagen networks [24]. For the mechanical analysis of reconstituted collagen matrices we used colloidal probes of 15 µm in diameter which is larger than the pore diameter of all investigated networks. Such an approach is necessary to access the micromechanical characteristics of networks, in contrast to other studies on the mechanics of single collagen fibrils [53] or macromechanical properties of collagen networks by rheometry [24, 54, 55]. By that, we are able to better probe local states of the somewhat heterogeneous collagen networks and to correlate it to differences in local cell response or to the distribution of data discussed above. On the other hand, we are confronted with relatively high standard deviations of our

measurements as a drawback of our approach. Nevertheless, the micromechanical analysis quite nicely shows that our new topological analysis provides a meaningful measure for the collagen networks characteristics.
A comparison of matrix topology, mechanics and cell invasion indicates an enhanced cell invasion into networks of smaller mesh size and with higher Young´s modulus. Interestingly, not the topology alone provides an indication of cell invasion behaviour in heterotypic collagen scaffolds, at least for the specific cell type investigated - namely fibroblasts. Obviously, the composition and thereby the different inner structure of these collagen fibrils result in different micromechanical properties of fibrillar networks and dictate an altered cell behaviour. As cell behaviour is frequently investigated in 3D collagen matrices with encapsulated cells, we want to point out, that our procedure is also suitable to analyse networks topology in this context. The automated analysis of network topology based on CFM and the analysis of network mechanics by colloidal probe can be applied with embedded cells as both methods can be used in localized way. This would be especially interesting, as it is known that fibrillogenesis is changed under such conditions due to variations in p*H*, buffer or proteins of serum-containing cell culture media.

5. Conclusion

In summary, we can conclude that we successfully reconstituted 3D composite collagen matrices with defined topological parameters including pore diameter, fibril diameter, fibril content, and isotropy of fibril orientation. The efficient algorithm can be used to characterize different kinds of networks and matrices investigated by different microscopy techniques as long as image data can be segmented into binary images.
The correlation of the quantified network topology to the mechanics of collagen networks as well as to the invasion of primary human dermal fibroblasts indicate the suitability of the introduced matrix reconstitution and topological analysis to better control cell behaviour in biomimetic cell culture scaffolds.
The straightforward and robust approach to fabricate and characterize collagen matrices of varying topology allows for further options of matrix modification like crosslinking or functionalization with other matrix components including glycosaminoglycans. Such experiments will allow the dissection of the impact of important parameters of ECM including topology, mechanics and mediator binding, which usually interfere with each other in cell studies.

Acknowledgements

L.K., U.A. and T.P. want to acknowledge financial support by the Deutsche Forschungsgemeinschaft (DFG, grant: SFB-TR67). K.F. and T.P. want to acknowledge financial support by ESF 'European Social Funds' and Free State of Saxony (grant: SAB 100140482). We gratefully acknowledge use of the imaging facility in the Magin lab, supported by DFG INST 268/230-1 to Thomas Magin.

Appendix A. Supplementary data

Supplementary data associated with this article can be found in the online version.

References

[1] Causa F, Netti PA, Ambrosio L. A multi-functional scaffold for tissue regeneration: the need to engineer a tissue analogue. Biomaterials 2007;28:5093-9.
[2] Hynes RO. The extracellular matrix: not just pretty fibrils. Science 2009;326:1216-9.
[3] Müller C, Müller A, Pompe T. Dissipative interactions in cell–matrix adhesion. Soft Matter 2013;9:6207-16.

[4] Chen CS, Mrksich M, Huang S, Whitesides GM, Ingber DE. Geometric control of cell life and death. Science 1997;276:1425-8.

[5] Cukierman E, Pankov R, Stevens DR, Yamada KM. Taking cell-matrix adhesions to the third dimension. Science 2001;294:1708-12.

[6] Beningo KA, Dembo M, Wang YL. Responses of fibroblasts to anchorage of dorsal extracellular matrix receptors. Proc Natl Acad Sci U S A 2004;101:18024-9.

[7] Kloxin AM, Kloxin CJ, Bowman CN, Anseth KS. Mechanical properties of cellularly responsive hydrogels and their experimental determination. Adv Mater 2010;22:3484-94.

[8] Lutolf MP, Hubbell JA. Synthetic biomaterials as instructive extracellular microenvironments for morphogenesis in tissue engineering. Nat Biotechnol 2005;23:47-55.

[9] Tsurkan MV, Chwalek K, Levental KR, Freudenberg U, Werner C. Modular StarPEG-Heparin Gels with Bifunctional Peptide Linkers. Macromol Rapid Commun 2010;31:1529-33.

[10] Bellis SL. Advantages of RGD peptides for directing cell association with biomaterials. Biomaterials 2011;32:4205-10.

[11] Collier JH, Segura T. Evolving the use of peptides as components of biomaterials. Biomaterials 2011;32:4198-204.

[12] Barker TH. The role of ECM proteins and protein fragments in guiding cell behavior in regenerative medicine. Biomaterials 2011;32:4211-4.

[13] Badylak SF, Freytes DO, Gilbert TW. Extracellular matrix as a biological scaffold material: Structure and function. Acta Biomater 2009;5:1-13.

[14] Szpaderska A, DiPietro L. In Vitro Matrigel Angiogenesis Model. In: DiPietro L, Burns A, editors. Wound Healing: Humana Press; 2003. p. 311-5.

[15] Miller JS, Stevens KR, Yang MT, Baker BM, Nguyen DH, Cohen DM, et al. Rapid casting of patterned vascular networks for perfusable engineered three-dimensional tissues. Nat Mater 2012;11:768-74.

[16] Birk D, Bruckner P. Collagen Suprastructures. In: Brinckmann J, Notbohm H, Müller PK, editors. Collagen: Springer Berlin Heidelberg; 2005. p. 185-205.

[17] Stamov D, Pompe T. Structure and function of ECM-based composite collagen I scaffolds. Soft Matter 2012;8:10200-12.

[18] Janmey PA, Winer JP, Weisel JW. Fibrin gels and their clinical and bioengineering applications. Journal of the Royal Society, Interface / the Royal Society 2009;6:1-10.

[19] Kirkpatrick CJ, Fuchs S, Unger RE. Co-culture systems for vascularization — Learning from nature. Advanced Drug Delivery Reviews 2011;63:291-9.

[20] Birk DE, Fitch JM, Linsenmayer TF. Organization of collagen types I and V in the embryonic chicken cornea. Invest Ophthalmol Vis Sci 1986;27:1470-7.

[21] Gathercole LJ, Keller A. Crimp morphology in the fibre-forming collagens. Matrix 1991;11:214-34.

[22] Kadler KE, Hill A, Canty-Laird EG. Collagen fibrillogenesis: fibronectin, integrins, and minor collagens as organizers and nucleators. Current Opinion in Cell Biology 2008;20:495-501.

[23] Wenstrup RJ, Smith SM, Florer JB, Zhang G, Beason DP, Seegmiller RE, et al. Regulation of Collagen Fibril Nucleation and Initial Fibril Assembly Involves Coordinate Interactions with Collagens V and XI in Developing Tendon. Journal of Biological Chemistry 2011;286:20455-65.

[24] Piechocka IK, van Oosten AS, Breuls RG, Koenderink GH. Rheology of heterotypic collagen networks. Biomacromolecules 2011;12:2797-805.

[25] Harris JR, Reiber A. Influence of saline and pH on collagen type I fibrillogenesis in vitro: Fibril polymorphism and colloidal gold labelling. Micron 2007;38:513-21.

[26] Roeder BA, Kokini K, Sturgis JE, Robinson JP, Voytik-Harbin SL. Tensile Mechanical Properties of Three-Dimensional Type I Collagen Extracellular Matrices With Varied Microstructure. Journal of Biomechanical Engineering 2002;124:214.

[27] Saeidi N, Karmelek KP, Paten JA, Zareian R, DiMasi E, Ruberti JW. Molecular crowding of collagen: a pathway to produce highly-organized collagenous structures. Biomaterials 2012;33:7366-74.

[28] Wolf K, Alexander S, Schacht V, Coussens LM, von Andrian UH, van Rheenen J, et al. Collagen-based cell migration models in vitro and in vivo. Seminars in Cell & Developmental Biology 2009;20:931-41.

[29] Raub CB, Unruh J, Suresh V, Krasieva T, Lindmo T, Gratton E, et al. Image Correlation Spectroscopy of Multiphoton Images Correlates with Collagen Mechanical Properties. Biophys J 2008;94:2361-73.

[30] Bayan C, Levitt JM, Miller E, Kaplan D, Georgakoudi I. Fully automated, quantitative, noninvasive assessment of collagen fiber content and organization in thick collagen gels. Journal of Applied Physics 2009;105:102042.

[31] Altendorf H, Decenciere E, Jeulin D, De sa Peixoto P, Deniset-Besseau A, Angelini E, et al. Imaging and 3D morphological analysis of collagen fibrils. Journal of microscopy 2012;247:161-75.

[32] Raub CB, Suresh V, Krasieva T, Lyubovitsky J, Mih JD, Putnam AJ, et al. Noninvasive Assessment of Collagen Gel Microstructure and Mechanics Using Multiphoton Microscopy. Biophys J 2007;92:2212-22.

[33] Brightman AO, Rajwa BP, Sturgis JE, McCallister ME, Robinson JP, Voytik-Harbin SL. Time-lapse confocal reflection microscopy of collagen fibrillogenesis and extracellular matrix assembly in vitro. Biopolymers 2000;54:222-34.

[34] Yang YL, Leone LM, Kaufman LJ. Elastic moduli of collagen gels can be predicted from two-dimensional confocal microscopy. Biophys J 2009;97:2051-60.

[35] D'Amore A, Stella JA, Wagner WR, Sacks MS. Characterization of the complete fiber network topology of planar fibrous tissues and scaffolds. Biomaterials 2010;31:5345-54.

[36] Gobeaux F, Mosser G, Anglo A, Panine P, Davidson P, Giraud-Guille MM, et al. Fibrillogenesis in Dense Collagen Solutions: A Physicochemical Study. Journal of Molecular Biology 2008;376:1509-22.

[37] Lindström SB, Vader DA, Kulachenko A, Weitz DA. Biopolymer network geometries: Characterization, regeneration, and elastic properties. Physical Review E 2010;82.

[38] Stein AM, Vader DA, Jawerth LM, Weitz DA, Sander LM. An algorithm for extracting the network geometry of three-dimensional collagen gels. Journal of Microscopy 2008;232:463-75.

[39] Mickel W, Münster S, Jawerth LM, Vader DA, Weitz DA, Sheppard AP, et al. Robust pore size analysis of filamentous networks from three-dimensional confocal microscopy. Biophys J 2008;95:6072-80.

[40] Lang NR, Münster S, Metzner C, Krauss P, Schurmann S, Lange J, et al. Estimating the 3D pore size distribution of biopolymer networks from directionally biased data. Biophys J 2013;105:1967-75.

[41] Jawerth LM, Munster S, Vader DA, Fabry B, Weitz DA. A blind spot in confocal reflection microscopy: the dependence of fiber brightness on fiber orientation in imaging biopolymer networks. Biophys J 2010;98:L1-3.

[42] Molteni M, Magatti D, Cardinali B, Rocco M, Ferri F. Fast two-dimensional bubble analysis of biopolymer filamentous networks pore size from confocal microscopy thin data stacks. Biophys J 2013;104:1160-9.

[43] Jiao Y, Torquato S. Quantitative characterization of the microstructure and transport properties of biopolymer networks. Phys Biol 2012;9:036009.

[44] Pompe T, Zschoche S, Herold N, Salchert K, Gouzy MF, Sperling C, et al. Maleic anhydride copolymers - a versatile platform for molecular biosurface engineering. Biomacromolecules 2003;4:1072-9.

[45] Douglas T, Heinemann S, Mietrach C, Hempel U, Bierbaum S, Scharnweber D, et al. Interactions of collagen types I and II with chondroitin sulfates A-C and their effect on osteoblast adhesion. Biomacromolecules 2007;8:1085-92.

[46] Hutter JL, Bechhoefer J. Calibration of atomic-force microscope tips. Review of Scientific Instruments 1993;64:1868.

[47] van der Smissen A, Samsonov S, Hintze V, Scharnweber D, Moeller S, Schnabelrauch M, et al. Artificial extracellular matrix composed of collagen I and high-sulfated hyaluronan interferes with TGFbeta signaling and prevents TGFbeta induced myofibroblast differentiation. Acta Biomater 2013.

[48] Buxboim A, Ivanovska IL, Discher DE. Matrix elasticity, cytoskeletal forces and physics of the nucleus: how deeply do cells 'feel' outside and in? J Cell Sci 2010;123:297-308.

[49] Friedl P, Wolf K. Plasticity of cell migration: a multiscale tuning model. J Cell Biol 2010;188:11-9.

[50] Wolf K, Te Lindert M, Krause M, Alexander S, Te Riet J, Willis AL, et al. Physical limits of cell migration: Control by ECM space and nuclear deformation and tuning by proteolysis and traction force. J Cell Biol 2013;201:1069-84.

[51] Carey SP, Kraning-Rush CM, Williams RM, Reinhart-King CA. Biophysical control of invasive tumor cell behavior by extracellular matrix microarchitecture. Biomaterials 2012;33:4157-65.

[52] Davison PF, Hong BS, Cannon DJ. Quantitative analysis of the collagens in the bovine cornea. Exp Eye Res 1979;29:97-107.

[53] Stamov DR, Khoa Nguyen TA, Evans HM, Pfohl T, Werner C, Pompe T. The impact of heparin intercalation at specific binding sites in telopeptide-free collagen type I fibrils. Biomaterials 2011;32:7444-53.

[54] Francis-Sedlak ME, Uriel S, Larson JC, Greisler HP, Venerus DC, Brey EM. Characterization of type I collagen gels modified by glycation. Biomaterials 2009;30:1851-6.

[55] Miron-Mendoza M, Seemann J, Grinnell F. The differential regulation of cell motile activity through matrix stiffness and porosity in three dimensional collagen matrices. Biomaterials 2010;31:6425-35.